Potential shift from a carbon sink to a source in Amazonian peatlands under a changing climate

Sirui Wang[a,b], Qianlai Zhuang[a,b,1], Outi Lähteenoja[c], Frederick C. Draper[d,e], and Hinsby Cadillo-Quiroz[c]

[a]Department of Earth, Atmospheric, and Planetary Sciences, Purdue University, West Lafayette, IN 47907; [b]Department of Agronomy, Purdue University, West Lafayette, IN 47907; [c]School of Life Sciences, Arizona State University, Tempe, AZ 85281; [d]Department of Global Ecology, Carnegie Institution for Science, Stanford, CA 94305; and [e]International Center for Tropical Botany, Florida International University, Miami, FL 33199

Edited by Carlos A. Nobre, Institute for Advanced Studies-University of São Paulo, Sao José dos Campos, Brazil, and approved October 18, 2018 (received for review January 24, 2018)

Amazonian peatlands store a large amount of soil organic carbon (SOC), and its fate under a future changing climate is unknown. Here, we use a process-based peatland biogeochemistry model to quantify the carbon accumulation for peatland and nonpeatland ecosystems in the Pastaza-Marañon foreland basin (PMFB) in the Peruvian Amazon from 12,000 y before present to AD 2100. Model simulations indicate that warming accelerates peat SOC loss, while increasing precipitation accelerates peat SOC accumulation at millennial time scales. The uncertain parameters and spatial variation of climate are significant sources of uncertainty to modeled peat carbon accumulation. Under warmer and presumably wetter conditions over the 21st century, SOC accumulation rate in the PMFB slows down to 7.9 (4.3–12.2) g·C·m^{-2}·y^{-1} from the current rate of 16.1 (9.1–23.7) g·C·m^{-2}·y^{-1}, and the region may turn into a carbon source to the atmosphere at −53.3 (−66.8 to −41.2) g·C·m^{-2}·y^{-1} (negative indicates source), depending on the level of warming. Peatland ecosystems show a higher vulnerability than nonpeatland ecosystems, as indicated by the ratio of their soil carbon density changes (ranging from 3.9 to 5.8). This is primarily due to larger peatlands carbon stocks and more dramatic responses of their aerobic and anaerobic decompositions in comparison with nonpeatland ecosystems under future climate conditions. Peatland and nonpeatland soils in the PMFB may lose up to 0.4 (0.32–0.52) Pg·C by AD 2100 with the largest loss from palm swamp. The carbon-dense Amazonian peatland may switch from a current carbon sink into a source in the 21st century.

peatland | modeling | climate | carbon | simulation

Tropical peatlands cover ∼441,025 km^2 and store a large quantity (88.6 Pg·C) of soil organic carbon (SOC) (1–4). These ecosystems occupy ∼11% of the global peatland area and account for 15–19% of the total global peat SOC stock (3). Tropical peatlands are mainly distributed in Southeast Asia (∼56%, 247,778 km^2) and South and Central America (∼23%, 107,486 km^2) (3). Recently, an additional 145,500 km^2 of tropical peatlands containing 30.6 Pg·C was discovered in the central Congo basin, Africa (5). Given their significant C stocks, studying their responses to past climatic trends and to the future climate change is of global importance (6–8).

To date, most studies on the role of tropical peatlands in the global C cycle have focused on Indonesian peatlands, which have been acting during the last decades as a considerable C source to the atmosphere resulting from anthropogenic activities (e.g., land exploitation and fires) (9–11). Few studies have focused on the Amazon basin, where peatlands remain nearly intact, and have been a long-term C sink (7, 8, 12, 13). The 120,000-km^2 Pastaza-Marañón foreland basin (PMFB) located in Peru is the most extensive peatland complex in the Amazon basin, with up to 7.5 m thick peat deposits. The basal ages vary from 0.67 to 8.9 ka (1 ka = 1,000 cal y before present) and the peat SOC accumulation rates range from 26 to 195 g·C·m^{-2}·y^{-1} (8, 14). It is a subsiding foreland basin, resulting from the Cenozoic uplift of the Andes Mountains (15–18) and characterized by meandering [>100 m in a year (19)] and avulsions of rivers [abrupt changes in the location of river stretches (20, 21)]. Waterlogged conditions due to high precipitation and low-lying topography provide a favorable environment for peat accumulation (13, 14). By measuring peat characteristics at several peatland sites within the basin, and using Landsat Thematic Mapper images, Lähteenoja et al. (14) estimated a peatland area of 21,929 km^2 with SOC stock of 3.116 Pg (0.837–9.461 Pg) for the central parts of the PMFB. Furthermore, by incorporating multisensor remote sensing and adding more peat core data, Draper et al. (13) mapped the distribution of peatland and nonpeatland ecosystems in the PMFB and estimated a peatland area of 35,600 ± 2,133 km^2 with 3.14 Pg·C (0.44–8.15 Pg) stored in the vegetation and peat deposits of the whole basin.

According to most climate models, mean air temperature of South America has been projected to increase by 1.8–5.1 °C for the PMFB by the end of this century (22–25). Annual precipitation is projected to increase by up to 500 mm, although a large uncertainty exists (22–25). The strong dependence of C dynamics on climate suggests that warming in the 21st century may turn the peatlands in the PMFB from a long-term C sink into a source (6, 7, 9, 26). However, this potential change has not been quantified or modeled in any way in previous studies. Nearly all models focusing on the future C dynamics of the Amazon basin have been applied to nonpeatland ecosystems (27–35) with the exception of ref. 29.

Process-based models offer an alternative approach to quantifying peatland C dynamics and providing insights for future projection (36–40). Recently, a peatland terrestrial ecosystem model (P-TEM) was developed for both peatland and nonpeatland ecosystems by combining a hydrology module (HM), a soil thermal module (STM), a methane dynamics module (MDM), and a

Significance

We use a process-based biogeochemistry model to quantify the carbon accumulation for peatland ecosystems in the Pastaza-Marañon foreland basin in the Peruvian Amazon from 12,000 y before present to AD 2100. We find that warming accelerates peat carbon loss, while increasing precipitation slightly enhances peat carbon accumulation at millennial time scales. With these impacts, our simulations suggest that the basin might lose up to 0.4 Pg·C by AD 2100, with the largest loss from palm swamp. If this loss rate is true for all Amazonia peatlands, we project that these carbon-dense peatlands may switch from a current carbon sink into a future source in this century.

Author contributions: S.W. and Q.Z. designed research; S.W., Q.Z., O.L., F.C.D., and H.C.-Q. performed research; S.W., Q.Z., O.L., F.C.D., and H.C.-Q. contributed new reagents/analytic tools; S.W., Q.Z., O.L., F.C.D., and H.C.-Q. analyzed data; and S.W., Q.Z., O.L., F.C.D., and H.C.-Q. wrote the paper.

The authors declare no conflict of interest.

This article is a PNAS Direct Submission.

[1]To whom correspondence should be addressed. Email: qzhuang@purdue.edu.

This article contains supporting information online at www.pnas.org/lookup/suppl/doi:10.1073/pnas.1801317115/-/DCSupplemental.

C and nitrogen dynamics module (CNDM) (39). P-TEM has been evaluated and used for estimating C stocks across the Alaskan landscape since the last deglaciation (39, 40). Here, we parameterize and evaluate the P-TEM for tropical peatlands and model the C dynamics of the peatlands in the PMFB, Peruvian Amazonia (Fig. 1) from 9 ka to AD 2014. The model parameters were optimized by using published peat, vegetation, and remote-sensing data for the PMFB from refs. 13 and 14 as well as other published sources (*SI Appendix*, Tables S1 and S2). The model was then used to (*i*) quantify past C accumulation from 12 ka to AD 2014 in peatlands and (*ii*) predict the future trends of C accumulation under different climate scenarios in the 21st century in peatland and nonpeatland ecosystems within the PMFB.

Past C Accumulation

The annual comparison between model simulation and measurements (14) at a temporal resolution of a year at the thickest and largest Amazonian peatland site (Aucayacu site) reveals that our model captures the historic peat SOC accumulation rates (Fig. 2*A*) and the peat depth profile (Fig. 2*B*) for most simulation periods, but overestimates the rates between 8 and 6 ka. Simulated total depth reaches 8 m (ranging 6–12 m), slightly higher than the measured 7.5 m (14). The correlation between simulations and measurements using 500-y bins at multiple sites with different vegetation types indicates that the model well estimates SOC accumulation trajectories at millennial time scales (*SI Appendix*, Fig. S1). The model underestimates the rates between 3 and 2 ka at San Jorge and between 0.5 and 0 ka at Charo. Although the model underestimates the rates between 2 and 1.5 ka at Rinon [an open peatland (OP) site], the starting basal age for the regional transient simulation for the OPs is at 1.6 ka (*SI Appendix*, Table S3). As indicated by the mean basal age applied in the model, pole forest (PF) has a longer SOC accumulation period than palm swamp (PS) and OP in general (*SI Appendix*, Fig. S1), with peat initiation of PF ∼2,000 y ahead of PS and OP peat initiation.

Our simulation suggests there were strong relationships between peat C dynamics and climatic change. Temporally, temperature and photosynthetically active radiation (PAR) rose slightly over the whole period (*SI Appendix*, Fig. S2 *A* and *E*), whereas annual precipitation decreased <4 ka and subsequently increased (*SI Appendix*, Fig. S2*C*). Under increasingly warmer and drier conditions <4 ka, the historic SOC accumulation rate declined at the Aucayacu site (Fig. 2*A*). It started to increase concurrently with the wetter conditions >3.5 ka (close to 4 ka), despite continuing warming. Overall, the historic SOC accumulation rates of the Aucayacu peat core followed the historic pattern of the precipitation change (*SI Appendix*, Fig. S2*C*). This suggests that higher rainfall might have accelerated while warming, and drought might have decelerated peat SOC accumulation at millennial time scales.

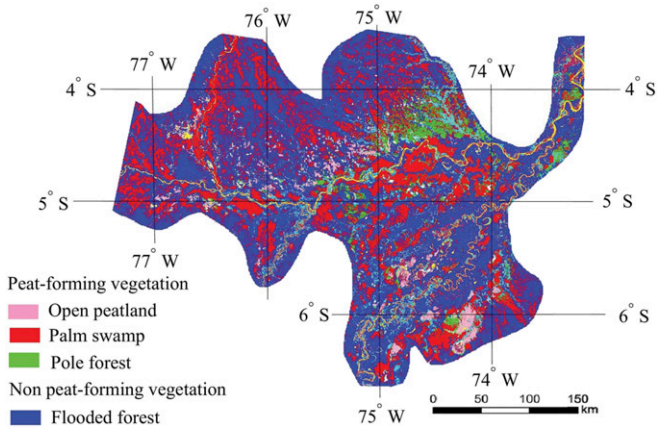

Fig. 1. Distribution of peat-forming and non-peat-forming vegetation in the PMFB at the resolution of 90 × 90 m (13). The map was resized to 1.69 × 1.69 km. Colors represent vegetation types: open peatland (pink), PS (red), PF (green), and FF (dark blue). Yellow represents open water, and light blue represents other. See figures 1 and 4 of ref. 13 for the original map.

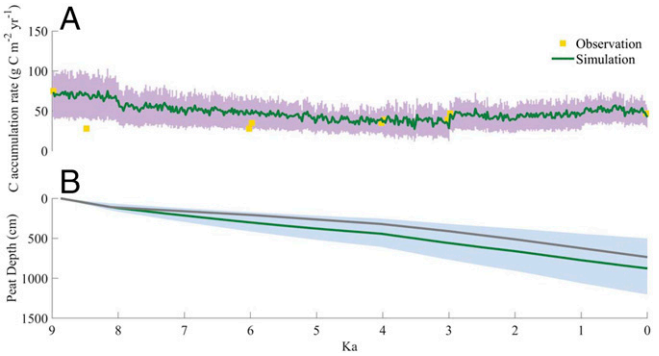

Fig. 2. Comparison between simulation and measurement (14) at the Aucayacu site: SOC accumulation rates (*A*) and peat depth (*B*). Shaded areas represent the range due to uncertainties from the posterior distributions of the parameters after the parameterization. A value of 0 cm at ∼9 ka indicates no peat accumulation.

Spatially, this relationship between the peat SOC accumulation and climate was indicated by the patterns of the peat SOC densities distribution and mean historic temperature and precipitation within the PMFB (Fig. 3 and *SI Appendix*, Fig. S3). We find that the highest peat SOC density region fell in the northeast with the highest precipitation and relatively low temperature. The secondary highest peat SOC region was located in the northwest with moderate precipitation but the lowest temperature. The lowest peat SOC zone fell within the southwest where the lowest precipitation and highest temperature coincided. This, again, suggests that higher precipitation increased, whereas higher temperature reduced peat SOC accumulation at regional scales.

The climatic effects on the long-term peat SOC accumulation in the PMFB can be explained by our simulated C fluxes and hydrological factors. Peat accumulated SOC where the rate of soil C input was higher than the decomposition (41). Soil C input from litters was largely controlled by and was proportional to plant net primary productivity (NPP). Soil decomposition was modeled as heterotrophic respiration (R_H) (42) (*SI Appendix*). Increasing temperature and PAR stimulated the plant C uptake by increasing NPP. However, warming might have created favorable conditions for microbial decomposition (43). Warming also increased the evapotranspiration, decreasing water table, thereby reducing anaerobic respiration and increasing aerobic respiration (44). Increasing precipitation had a positive effect on NPP. It also lifted the water table and decreased R_H. This, in turn, enhanced peat C accumulation. In our previous study for the northern (Alaskan) peatlands (40), under the warmer conditions, the stimulation of NPP exceeded the stimulation of R_H, thereby increasing SOC accumulation in northern peatlands during the Holocene Thermal Maximum (HTM). Similarly, we find that R_H within 1-m depth followed the increasing trend of temperature with a decrease at 4 ka when precipitation increased (*SI Appendix*, Fig. S4*B*). This suggests that warmer condition in the PMFB enhances R_H while wetter condition decreases R_H. The volumetric soil moisture (VSM) (*SI Appendix*, Fig. S4*C*) and water table (*SI Appendix*, Fig. S4*D*) started decreasing at 8 ka as precipitation became lower. At the same time, R_H kept increasing under such drier condition. Interestingly, when climate became wetter at ∼4 ka (*SI Appendix*, Fig. S2*C*), the VSM abruptly increased. The water table also stopped dropping and showed an increase pattern. Meanwhile, R_H started decreasing. This again suggests that higher precipitation may decrease R_H and thus slows the peat SOC decomposition by increasing the soil moisture and raising the water table. As warming continued, the increase of VSM and water table were slight, presumably due to the enhanced evapotranspiration.

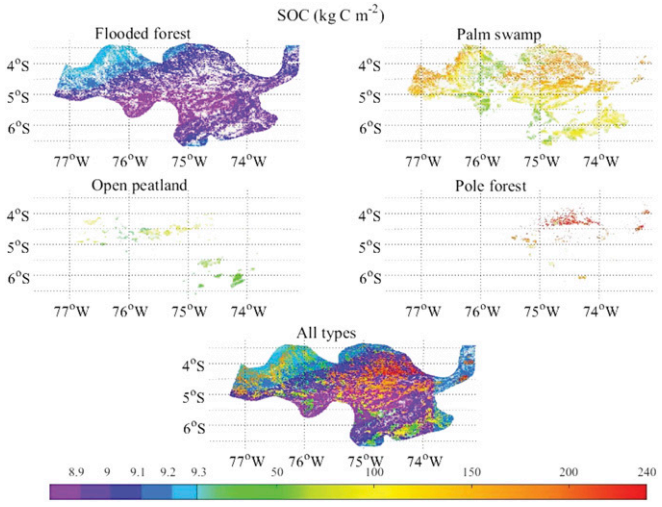

Fig. 3. Current (AD 2014) SOC density of FF, PS, open peatland, PF, and their combination in the PMFB.

To examine how temperature and precipitation have impacted NPP in this region. The attributions of these two key drivers and soil water content to NPP for both historical periods and the 21st century were analyzed with the analysis of variance (ANOVA) table and the F-test of the multivariate linear regression between annual mean NPP and climate variables. For the historical simulation at Aucayacu site, we find that, although higher precipitation and higher temperature increase the NPP (*SI Appendix*, Tables S4 and S5), those two factors have limited effects presumably because the temperature exceeds the optimum temperature for photosynthesis and soil water content is already suitable for plant growth. The variable with the highest importance is VSM, indicating that the hydrological condition plays the most important role in determining the NPP. Such hydrological condition is modeled by various factors including the temperature, precipitation, solar radiation, and others such as soil porosity, soil layer characteristics that are described in our previous hydrological modeling studies (39, 40).

Our historical simulations at Aucayacu and in the PMFB suggest that NPP was consistent with the temporal patterns of precipitation and VSM (*SI Appendix*, Fig. S2*C*). The spatial correlations between NPP, vegetation C density, and mean historic precipitation were detected (*SI Appendix*, Figs. S3*B* and S5) when observing each peatland vegetation type separately. Pixels with higher vegetation C density and NPP fell within the northeastern wetter region, while lower vegetation C density and NPP pixels were in the southwestern drier region. Our explanation is that during the historical period, the point where NPP will no longer positively respond to the increasing precipitation and VSM has not been reached. Still, the wetter condition stimulates the SOC accumulation by increasing NPP and decreasing R_H. However, for the simulations under three future climate scenarios (*SI Appendix*, Table S6), we find that the F values of the precipitation started decreasing as the precipitation continued to be higher from Representative Concentration Pathway (RCP) 2.6 to 8.5. This suggests that precipitation becomes less and less important in the future for NPP as it increases, based on the existing suitable hydrological condition.

In our model, GPP is a function of atmospheric CO_2 concentrations in addition to physical variables (*SI Appendix*). The CO_2 effects is modeled with a Michaelis–Menten equation considering CO_2 concentrations inside leaves which is assumed to be directly proportional to atmospheric CO_2 concentrations when stomata are fully open. When moisture is a limiting factor, the limitation on CO_2 assimilation is modeled by modifying the conductance of leaves to CO_2 diffusion. The moisture availability is expressed as the ratio of actual evapotranspiration (*EET*) to potential evapotranspiration (*PET*). The relationship between CO_2 concentration inside stomatal cavities (C_i) and in the atmosphere (C_a) is proportional to relative moisture availability:

$$G_V = 0.1 + \left(\frac{0.9\,EET}{PET}\right)$$

$$C_i = G_V C_a,$$

where G_V is a unitless multiplier that accounts for changes in leaf conductivity to CO_2 resulting from changes in moisture availability. When there is sufficient water in soils, *EET* will not be limited by water, which will reach its maximum value, GV is close to 1. This suggests that inside of leaves, CO_2 will be close to ambient CO_2. When the ecosystem has sufficient precipitation, GPP and NPP will not respond to increasing precipitation.

At northern high latitudes, in addition to CO_2 fertilization effects, warming also enhances photosynthesis, stimulating plant productivity (NPP) and thus increasing SOC accumulation (42, 45–47). In contrast, warming in the tropical regions generally led to temperatures above the optimum level for photosynthesis (48, 49), which is also suggested by the ANOVA (*SI Appendix*, Tables S4 and S6), as increasing temperature in the future has less and less positive effects on NPP. Increasing temperature accelerates R_H, however, at the same time. The less sensitivity of NPP vs. R_H to warming might ultimately result in the SOC loss in the PMFB under warmer conditions.

However, hydrology, NPP, and SOC accumulation can also be controlled by autogenic processes of peatlands such as transition from minerotrophic to ombrotrophic conditions (8). This transition is largely induced by the form and thickness of the peat deposit and less affected by prevailing climatic conditions—as long as the rainfall is sufficient to sustain an rain-fed bog. Interestingly, in the Aucayacu peatland, the transition from minerotrophic to ombrotrophic conditions occurred ∼4 ka (3.5 ka)—exactly when precipitation started to increase. It might have been a coincidence, but it is also possible that the increased precipitation enabled the appearance of ombrotrophic bogs. If this is the case, a change in the precipitation did not affect the NPP directly but indirectly by inducing a change in the peatland type. Since our model cannot simulate the paleo-ecological change including the shifts between different peatland ecosystem types through time, our results may only partly explain the observed patterns, with much information still relying on paleo-ecological studies (14, 50–52). The relationship between NPP and precipitation for peatland ecosystems in the region should be further studied in the future.

Another key control of the current distribution of peat depths and SOC densities within the PMFB is the active lateral migration of rivers (14). The current distribution of peat SOC densities can be explained by both climatic and geological factors. The Amazon river networks can be affected under future climate conditions, which will affect peatland dynamics (e.g., formation and area change). Furthermore , our model did not differentiate the minerotrophic vs. ombrotrophic conditions for the peatland ecosystems, which will introduce biases. Incorporating these dynamics into future analysis shall improve our predictions of SOC for this region.

Our uncertainty analysis suggests that the uncertainty of the simulated past C accumulation rates was mainly due to parameters, spatial variations of climate variables (*SI Appendix*, Fig. S3), and the uncertain peat basal ages (*SI Appendix*, Table S3). Specifically, using the mean peat basal age by averaging the basal ages of peat samples for each peatland type is a top uncertainty source. The variation of peat characteristics (e.g., bulk density, C content, and peat depth) and limited number of samples are also sources of the uncertainty.

Current C Stocks

Overall, model simulations of current peatland C stocks are comparable to the field measurements of ref. 13. Specifically, PF has the SOC density of 1,900 Mg·C·ha^{-1}, consistent with the field measurements (800–2,200 Mg·C·ha^{-1}; *SI Appendix*, Fig. S6*A*) (13). PS has the next highest SOC density (1,100 Mg·C·ha^{-1}),

which is sufficiently within the measured range of 300–1,390 Mg·C·ha^{-1}. The SOC density of OP is 535 Mg·C·ha^{-1}, also within the measured 392–1,492 Mg·C·ha^{-1}. The high SOC density of PF corresponds to the longer SOC accumulation period compared with the other types (*SI Appendix*, Figs. S1 *A* and *B* and S6*A*). Our simulations are even closer to the field measurements (13) when vegetation C density was examined (*SI Appendix*, Fig. S6*B*). The simulated lowest vegetation C density was in PF (86 Mg·C·ha^{-1}) and within the measured range of 80–100 Mg·C·ha^{-1}.

The model estimates a total SOC of 3.922 (2.208–5.777) Pg in the PMFB including 3.519 (1.833–5.344) Pg in the peatland soils, which is higher than the measured total peat SOC, 2.844 Pg (*SI Appendix*, Table S7) (13). The simulated vegetation C stock of 1.104 (1.097–1.137) Pg with 0.34 (0.338–0.369) Pg on the PMFB peatlands is also higher than the measured value (0.293 Pg·C) (13). Our model may overestimate the soil and vegetation C stocks. The uncertainty of the simulated C stocks is mainly due to the spatial variations of the interpolated mean temperature (25–29 °C) and precipitation (2,200–2,900 mm) (*SI Appendix*, Fig. S3).

Future Projection

Under the RCP 2.6 scenario (see below for climate description), the SOC accumulation rate in all ecosystem types within the PMFB decreases from 16 (9–24) to 7.9 (4.3–12.2) g·C·m^{-2}·y^{-1}, and the SOC accumulation rate in the peatlands dramatically decreases from 56 (29–85) to 23 (15–32) g·C·m^{-2}·y^{-1} (Table 1). The PS exhibits the biggest drop from 65 to 26 g·C·m^{-2}·y^{-1}. Spatially, the majority of pixels within the PMFB have positive SOC accumulation and vegetation C change, but some areas with PS have SOC loss (Fig. 4 and *SI Appendix*, Fig. S7). Overall, 0.067 (0.037–0.108) Pg SOC, including 0.06 (0.03–0.1) Pg SOC in the peatlands, will be accumulated in the PMFB by the end of the 21st century under moderately warmer and wetter conditions of this climate scenario (Table 1). There will be 0.0148 Pg·C accumulated in vegetation, including 0.0048 Pg·C in peatland vegetation.

Under the RCP 8.5 scenario, the SOC accumulation rate declines from 16 to −53 (−67 to approximately −41) C·m^{-2}·y^{-1}, and the rate in peatlands declines from 56 to −123 (−152 to approximately −91) C·m^{-2}·y^{-1} (Table 1). Again, the highest decline of the rate is for PS, from 65 to −135 g·C·m^{-2}·y^{-1}. The pixels with SOC and vegetation C loss dominate the region (Fig. 4 and *SI Appendix*, Fig. S7). Under this climate scenario, the PMFB will act as a C source of 0.413 (0.319–0.518) Pg·C by AD 2100 (Table 1). Peatlands will lose 0.31 (0.23–0.38) Pg·C compared with 0.1 Pg·C loss from nonpeatland ecosystems. Vegetation will lose 0.07 Pg·C, including 0.02 Pg·C from peatland vegetation. Among all peatland ecosystem types, PS could be severely affected by the climate due to its large area within the PMFB and within the whole Amazon Basin (53). It must be taken into account that the tendency of the model to overestimate the current soil and vegetation C stocks in the PMFB (*SI Appendix*, Table S7) might affect these values to some extent.

Under the intermediate RCP 4.5 scenario, the SOC accumulation rate declines from 16 to −19 C·m^{-2}·y^{-1} and the SOC accumulation rate in peatlands declines from 56 to −45 C·m^{-2}·y^{-1}. Peatlands will lose 0.12 Pg·C compared with 0.034 Pg·C from nonpeatlands.

Three extra simulations were conducted as sensitivity tests to examine the effects of potential drier climate in the PFMB on SOC accumulation rates. We assume that (*i*) the future precipitation will decrease 5% in our study region over the century, but holding air temperature change as in the original RCP 2.6; (*ii*) the future precipitation will decrease 10% but holding air temperature change as in RCP 4.5; and (*iii*) the future precipitation will decrease 15% but holding air temperature change as in RCP 8.5. The precipitation was manually decreased at monthly step for each grid cell from AD 2014 to AD 2100 to achieve the certain percentage total reduction at the end of AD 2100. Our simulations show that the C accumulations are +0.027 (0.02–0.068), −0.203 (−0.349 to approximately −0.167), and −0.594 (−0.731 to approximately −0.51) Pg·C under the three sensitivity simulations (Table 2). These extra simulations suggest that the slightly drier condition will decrease but will not have significant effects on the C accumulation in this region.

The modeled current C stocks agree with the field observations at the Aucayacu site, which is a PF site. However, instead of PF, PS is the dominant peatland type in the study area, and its SOC accumulation rates at the Charo site is underestimated. Thus, using PS as representative peatland types for regional simulations under future climate scenarios may evolve uncertainty due to the underestimation during the parameterization.

Table 1. Current SOC accumulation rates, soil and vegetation C stocks, and their changes in the PMFB from AD 2014 to 2100 in RCP 2.6 and RCP 8.5 scenarios (see RCP 4.5 in *Future Projection*)

	Soil C accumulation rates, g·C·m^{-2}·y^{-1}			SOC, Pg			Vegetation C, Pg		
Ecosystem type	Current	RCP 2.6	RCP 8.5	Current	RCP 2.6	RCP 8.5	Current	RCP 2.6	RCP 8.5
PF									
Mean	15.02	11.88	−89.95	0.511	+0.003	−0.023	0.022	+0.0004	−0.0021
Range	7.9–18.9	6.3–14.5	−135.3, −56.7	0.269–0.646	0.0016–0.0037	−0.035, −0.015	0.0215–0.0218		
PSs									
Mean	64.69	26.09	−135.23	2.779	+0.052	−0.264	0.318	+0.0044	−0.02
Range	34–101.8	15.2–43.9	−160.4, −102	1.459–4.376	0.03–0.09	−0.313, −0.199	0.316–0.349		
OPs									
Mean	29.53	14.69	−63.84	0.229	+0.005	−0.022	~0	~0	~0
Range	13.5–41.5	8–17.3	−98.2, −40.9	0.105–0.322	0.0027–0.0059	−0.034, −0.014	~0		
Nonpeatland									
Mean	0.1	1.64	−25.22	0.403	+0.007	−0.104	0.764	+0.01	−0.0482
Range	0.09–0.11	1.54–1.76	−32.8, −22.1	0.375–0.433	0.0066–0.0075	−0.136, −0.091	0.759–0.768		
Total (peatlands)									
Mean	55.98	23.42	−122.7	3.519	+0.06	−0.309	0.34	+0.0048	−0.0221
Range	29.1–85	14.9–31.5	−151.7, −90.5	1.833–5.344	0.03–0.1	−0.382, −0.228	0.338–0.369		
Peatlands+ nonpeatland									
Mean	16.08	7.89	−53.25	3.922	+0.067	−0.413	1.104	+0.0148	−0.0703
Range	9.1–23.7	4.3–12.2	−66.82, −41.2	2.208–5.777	0.037–0.108	−0.518, −0.319	1.097–1.137		

Current soil organic accumulation rates are mean rates and uncertainty ranges over the simulation periods till AD 2014 and total rates are area-weighted means. The uncertainty ranges of the "simulation" are from the uncertainty of the parameterization plus the uncertainty from the climate data interpolation. "+" and "−" in SOC and vegetation C columns indicate C accumulation and loss the from AD 2014 to AD 2100.

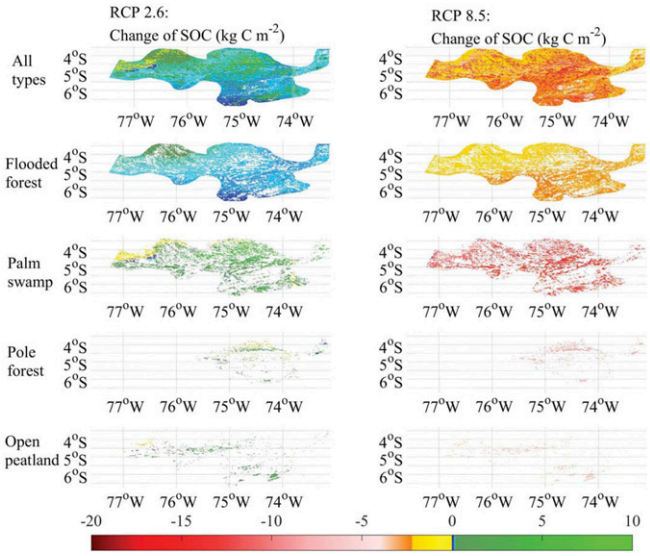

Fig. 4. Changes of SOC density from AD 2014 to 2100 under RCP 2.6 and RCP 8.5 future climate scenarios in FF, PS, PF, open peatland, and their combination in the PMFB. Blue and green represent the SOC accumulation. Yellow and red represent the SOC loss.

In conclusion, the warming in the 21st century may weaken the C sink function of the Amazonian peatlands in the PMFB or may entirely switch them from a long-term carbon sink into a source, depending on the severity of the warming. The same has also been predicted for the Amazonian rainforest in general (26). The vegetation and SOC density changes [future total C stock changes (Table 1) divided by the corresponding areas (*SI Appendix*, Table S7) of peatlands and nonpeatland] were calculated to compare with other studies. Our model estimation of vegetation C change for the nonpeatland [mainly flooded forest (FF)] ecosystem in the 21st century (+0.23 to approximately −1.17 kg·C·m^{-2}) is well within the range of other studies (+0.6 to approximately −1.2 kg·C·m^{-2}) on the future vegetation C change from Amazonian rainforest dieback (26, 54) (*SI Appendix*, Table S8). Our estimation of SOC change for the nonpeatland ecosystem in the 21st century (+0.18 to approximately −3.35 kg·C·m^{-2}) is also comparable to −3.88 kg·C·m^{-2} from other studies (26, 54). Furthermore, we find that the ratio of SOC density changes for peatlands and nonpeatland ecosystems in the next 100 y ranges from 3.9 to 5.8 (*SI Appendix*, Table S8). This indicates that future warming is likely to affect the Amazonian peatlands more dramatically than nonpeatland ecosystems, although the total area of peatlands is much smaller than that of nonpeatland ecosystems within the PMFB (31,000 vs. 47,000 km^2; see *SI Appendix* for areas). The high vulnerability of peatland ecosystems to future climate is presumably due to its large amount of existing SOC stock (3.5 Pg·C) compared with nonpeatland ecosystems (0.4 Pg·C). Another possible reason is that, in addition to the nonlinear function defining the VSM effect on heterotrophic respiration within the unsaturated zone, there is also a linear relation between water-table depth and aerobic respiration in the model (see *SI Appendix* for decomposition calculation). Future warming increases evapotranspiration that subsequently decreases VSM and increases aerobic respiration for both peatland and nonpeatland ecosystems. For peatlands, it further lowers the water table which, in turn, increases aerobic respiration. This suggests that peatland ecosystems may suffer larger SOC decomposition under the changing climate and may help explain its vulnerability. In addition, increased land use change, expansion of commercial agriculture, transport infrastructure, and hydropower development form a threat to the persistence of the considerable C stock (55). The most carbon dense ecosystems of the whole Amazon basin may turn into C sources.

Methods

The Peatland Biogeochemistry Model and Its Parameterization. In P-TEM, peat SOC accumulation is determined by the difference between NPP and aerobic and anaerobic respiration R_H at a monthly step (see refs. 1 and 2 and *SI Appendix* for model details). Parameters in P-TEM were first optimized with data of annual C fluxes and stocks in the Amazon basin taken from literature (*SI Appendix*, Table S1) to obtain the prior distribution of the parameter space for peatland ecosystems (see *SI Appendix* for details) Specifically, site-level measurements of tree biomass from Amazonian peatlands (13) were used to compare with model simulations to optimize parameters. Due to the lack of NPP measurements, NPP values used in the model are field measurements from neighboring white-sand forests (for PF peatlands) and seasonally FFs (for PS peatlands and flooded forests) (*SI Appendix*, Table S1). Second, a Bayesian approach was used to optimize parameters (*SI Appendix*, Table S2) with Monte Carlo ensemble simulations driven by the extracted paleo climate data (*SI Appendix*, Fig. S2) at five peatland sites (*SI Appendix*, Fig. S1).

The distribution of vegetation types was taken from ref. 13 at a resolution of 90 × 90 m and was resized to 1.69 × 1.69 km. Vegetation types in the region include three peat-forming vegetation types [PF, PS, and OP (peatland lacking closed canopy)] and a nonpeat forming type [flooded forest (FF)] (Fig. 1). OP was assumed to have minimal NPP and vegetation biomass during the simulation (13).

Climate Data. The climate forcing data for historic simulations include temperature, precipitation, PAR, vapor pressure at a monthly step, and CO_2 at an annual step from 12 ka to AD 1990, simulated by CCSM3 (TraCE-21ka) at a spatial resolution of 3.75° × 3.75°. Climate-forcing data for modern simulations is from the Climate Research Unit (CRU2.0) at a monthly step from AD 1990 to 2014 at a resolution of 0.5° × 0.5°. For future simulations, we applied the RCP 2.6 [mean annual temperature in the PMFB has the smallest increase (by ∼0.5 °C), mean annual precipitation increases by ∼260 mm, and CO_2 increases by ∼80 ppm at 2050 AD and decreases by ∼30 ppm at AD 2100],

Table 2. Current SOC accumulation rates, soil and vegetation C stocks, and their changes in the PMFB from AD 2014 to 2100 in the sensitivity tests

Sensitivity tests	Soil C accumulation rates, g·C·m^{-2}·y^{-1}			SOC, Pg			Vegetation C, Pg		
	Current	−5%	−15%	Current	−5%	−15%	Current	−5%	−15%
Peatlands									
Mean	55.98	13.92	−163.13	3.519	+0.03	−0.425	0.34	+0.0043	−0.0257
Range	29.1–85	8.9–18.86	−205.1, −146	1.833–5.344	0.01–0.6	−0.544–0.398	0.338–0.369		
Peatlands+ nonpeatland									
Mean	16.08	4.45	−76.75	3.922	+0.027	−0.594	1.104	+0.0124	−0.0758
Range	9.1–23.7	2.3–7.91	−94.33, −65.8	2.208–5.777	0.02–0.068	−0.731, −0.51	1.097–1.137		

Current soil organic accumulation rates are mean rates and uncertainty ranges over the simulation periods till AD 2014 and total rates are area-weighted means. The uncertainty ranges of the "simulation" are from the uncertainty of the parameterization plus the uncertainty from the climate data interpolation. "+" and "−" in SOC and vegetation C columns indicate C accumulation and loss in from AD 2014 to AD 2100. "−5%" and "−15%" in sensitivity tests indicate 5% and 15% annual precipitation reduction by 2100 AD under RCP 2.6 and RCP 8.5.

RCP 4.5 (by ~1.5 °C, ~290 mm, and CO_2 increases by ~150 ppm at AD 2100), and RCP 8.5 (by ~2.7 °C , ~350 mm, and ~600 ppm at AD 2100) at a monthly step from AD 2014 to 2100 at 0.5° × 0.5° as possible future climate scenarios. The CRU data together with the modern digital elevation data at 1.69 × 1.69 km were input into interpolation software ANUSPLIN4.4. We then downscaled the paleo-climate data (TraCE-21ka, 3.75° × 3.75°) and the RCP data (0.5° × 0.5°) based on the spatial variations of the interpolated CRU data (1.69 × 1.69 km) by assuming that the spatial variations of CRU to be the same as that of paleo and RCP data.

Model Application and Uncertainty Analysis. A 500-y run was conducted for each peatland ecosystem type ahead of the basal age by using parameters of non-peat-forming FF to determine the initial SOC within the upper 1-m mineral soil underlying the peat deposit. The model was first run from 12 ka to AD 2014 for validation at five peatland sites (*SI Appendix*, Fig. S1). The simulated SOC accumulation rates of PS, OP, and PF were first compared with measured SOC accumulation rates (7, 14) annually in 500-y bins. Second, we applied the model to a regional simulation with interpolated monthly paleo-climate data for the PMFB. We averaged all of the measured basal ages of each peatland type to determine the mean basal age of each peatland ecosystem type (*SI Appendix*, Table S3). Basal ages at sites where they have not been measured were calculated by using mean SOC accumulation rates, bulk density, peat depth, and C content of each peatland ecosystem type derived from refs. 7, 13, and 14, following the equations in ref. 7. We conducted the simulation from 1 ka to AD 2014 for FF. Finally, we conducted the simulations for future projection using the interpolated RCP 2.6, RCP 4.5, and RCP 8.5. A series of simulations were conducted to examine the effects of the spatial variation of climate and the posterior distribution of the parameter on the estimated C accumulation rates and stocks (see *SI Appendix* for details). Twenty sets of parameters were randomly drawn from the posterior parameter space. All pixels in the study area were then assigned with the same climate forcing data which were random combinations between temperature and precipitation.

1. Page SE, et al. (2002) The amount of carbon released from peat and forest fires in Indonesia during 1997. *Nature* 420:61–65.
2. Page SE, et al. (2004) A record of Late Pleistocene and Holocene carbon accumulation and climate change from an equatorial peat bog (Kalimantan, Indonesia): Implications for past, present and future carbon dynamics. *J Quat Sci* 19:625–635.
3. Page SE, et al. (2011) Global and regional importance of the tropical peatland carbon pool. *Glob Change Biol* 17:798–818.
4. Rieley JO, et al. (2008) Tropical peatlands: carbon stores, carbon gas emissions and contribution to climate change processes. *Peatlands and Climate Change*, ed Strack M (International Peatland Society, Laskunet, Finland), pp 148–182.
5. Dargie GC, et al. (2017) Age, extent and carbon storage of the central Congo Basin peatland complex. *Nature* 542:86–90.
6. Guzmán Castillo W (2007) Valor económico del manejo sostenible de los ecosistemas de aguaje (Mauritia flexuosa). *International Congress on Development, Environment and Natural Resources: Multi-Level and Multi-Scale Sustainability*, eds Feyen J, Aguirre LF, Moraes M (Universidad Mayor San Simón, Cochabamba, Bolivia), Vol 3, pp 1513–1521.
7. Lähteenoja O, et al. (2009a) Amazonian peatlands: An ignored C sink and potential source. *Glob Change Biol* 15:2311–2320.
8. Lähteenoja O, Page S (2011) High diversity of tropical peatland ecosystem types in the Pastaza-Marañón basin, Peruvian Amazonia. *J Geophys Res Biogeosci* 116:G02025.
9. Rieley JO, Page SE (2005) *Wise Use of Tropical Peatlands: Focus on Southeast Asia: Synthesis of Results and Conclusions of the UK Darwin Initiative and the EU INCO EUTROP, STRAPEAT and RESTORPEAT Partnerships Together with Proposals for Implementing Wise Use of Tropical Peatlands*, ed Jauhiainen J (ALTERRA, Wageningen, The Netherlands).
10. Maltby E, et al. (1993) Carbon dynamics in peatlands and other wetland soils regional and global perspectives. *Chemosphere* 27:999–1023.
11. Miettinen J, et al. (2011) Two decades of destruction in Southeast Asia's peat swamp forests. *Front Ecol Environ* 10:124–128.
12. Lähteenoja O, et al. (2009b) Amazonian floodplains harbour minerotrophic and ombrotrophic peatlands. *Catena* 79:140–145.
13. Draper FC, et al. (2014) The distribution and amount of carbon in the largest peatland complex in Amazonia. *Environ Res Lett* 9:124017.
14. Lähteenoja O, et al. (2012) The large Amazonian peatland carbon sink in the subsiding Pastaza-Marañón foreland basin, Peru. *Glob Change Biol* 18:164–178.
15. Dumont JF, et al. (1990) Wetland and upland forest ecosystems in Peruvian Amazonia: Plant species diversity in the light of some geological and botanical evidence. *For Ecol Manage* 33:125–139.
16. Dumont JF, et al. (1991) Morphostructural provinces and neotectonics in the Amazonian lowlands of Peru. *J South Am Earth Sci* 4:373–381.
17. Räsänen ME, et al. (1990) Evolution of the western Amazon lowland relief: Impact of Andean foreland dynamics. *Terra Nova* 2:320–332.
18. Räsänen ME, et al. (1992) Recent and ancient fluvial deposition systems in the Amazonian foreland basin, Peru. *Geol Mag* 129:293–306.
19. Kalliola, et al. (1992) Upper Amazon channel migration: Implications for vegetation perturbance and succession using bitemporal Landsat images. *Naturwissenschaften* 79:75–79.
20. Smith ND, et al. (1989) Anatomy of an avulsion. *Sedimentology* 36:1–23.
21. Neller RJ, et al. (1992) On the formation of blocked valley lakes by channel avulsion in Upper Amazon foreland basins. *Z Geomorphol* 36:401–411.
22. Guimberteau M, et al. (2013) Future changes in precipitation and impacts on extreme streamflow over Amazonian sub-basins. *Environ Res Lett* 8:014035.
23. Marengo JA, et al. (2012) Development of regional future climate change scenarios in South America using the Eta CPTEC/HadCM3 climate change projections: Climatology and regional analyses for the Amazon, São Francisco and the Parana River Basins. *Clim Dyn* 38:1829–1848.
24. Sánchez E, et al. (2015) Regional climate modelling in CLARIS-LPB: A concerted approach towards twenty first century projections of regional temperature and precipitation over South America. *Clim Dyn* 45:2193–2212.
25. Zulkafli Z, et al. (2016) Projected increases in the annual flood pulse of the Western Amazon. *Environ Res Lett* 11:014013.
26. Cox PM, et al. (2004) Amazonian forest dieback under climate-carbon cycle projections for the 21st century. *Theor Appl Climatol* 78:137–156.
27. Tian H, et al. (1998) Effect of interannual climate variability on carbon storage in Amazonian ecosystems. *Nature* 396:664–667.
28. Tian H, et al. (2000) Climatic and biotic controls on annual carbon storage in Amazonian ecosystems. *Glob Ecol Biogeogr* 9:315–335.
29. Li W, et al. (2007) Future precipitation changes and their implications for tropical peatlands. *Geophys Res Lett* 34:L01403.
30. Cleveland CC, et al. (2015) A comparison of plot-based satellite and Earth system model estimates of tropical forest net primary production. *Global Biogeochem Cycles* 29:626–644.
31. Rowland L, et al. (2015) Modelling climate change responses in tropical forests: Similar productivity estimates across five models, but different mechanisms and responses. *Geosci Model Dev* 8:1097–1110.
32. Restrepo-Coupe N, et al. (2017) Do dynamic global vegetation models capture the seasonality of carbon fluxes in the Amazon basin? A data-model intercomparison. *Glob Change Biol* 23:191–208.
33. Powell TL, et al. (2013) Confronting model predictions of carbon fluxes with measurements of Amazon forests subjected to experimental drought. *New Phytol* 200:350–365.
34. Delbart N, et al. (2010) Mortality as a key driver of the spatial distribution of aboveground biomass in Amazonian forest: Results from a dynamic vegetation model. *Biogeosciences* 7:3027–3039.
35. Schulman L, et al. (1999) Parameters for global ecosystem models. *Nature* 399:535–536.
36. Frolking S, et al. (2010) A new model of Holocene peatland net primary production, decomposition, water balance, and peat accumulation. *Earth Syst Dyn* 1:1–21.
37. Spahni R, et al. (2013) Transient simulations of the carbon and nitrogen dynamics in northern peatlands: From the Last Glacial Maximum to the 21st century. *Clim Past* 9:1287–1308.
38. Kleinen T, et al. (2012) A dynamic model of wetland extent and peat accumulation: Results for the Holocene. *Biogeosciences* 9:235–248.
39. Wang S, et al. (2016a) Quantifying peat carbon accumulation in Alaska using a process-based biogeochemistry model. *J Geophys Res Biogeosci* 121:2172–2185.
40. Wang S, et al. (2016b) Quantifying soil carbon accumulation in Alaskan terrestrial ecosystems during the last 15000 years. *Biogeosciences* 13:6305–6319.
41. Loisel J, et al. (2012) Global-scale pattern of peatland Sphagnum growth driven by photosynthetically active radiation and growing season length. *Biogeosciences* 9:2737–2746.
42. Yu Z, et al. (2009) Sensitivity of northern peatland carbon dynamics to Holocene climate change. *Carbon Cycling in Northern Peatlands*, eds Baird AJ et al., Geophysical Monograph Series (American Geophysical Union, Washington, DC), vol 184, pp 55–69.
43. Nobrega S, et al. (2007) Deeper snow enhances winter respiration from both plant-associated and bulk soil carbon pools in birch hummock tundra. *Ecosystems* 10:419–431.
44. Hobbie SE, et al. (2000) Controls over carbon storage and turnover in high latitude soils. *Glob Change Biol* 6:196–210.
45. Davidson EA, Janssens IA (2006) Temperature sensitivity of soil carbon decomposition and feedbacks to climate change. *Nature* 440:165–173.
46. Jones MC, Yu Z (2010) Rapid deglacial and early Holocene expansion of peatlands in Alaska. *Proc Natl Acad Sci USA* 107:7347–7352.
47. Yu Z, et al. (2010) Global peatland dynamics since the Last Glacial Maximum. *Geophys Res Lett* 37:L13402.
48. Jenkinson DS, et al. (1991) Model estimates of CO(2) emissions from soil in response to global warming. *Nature* 351:304–306.
49. Cox PM, et al. (2002) Modelling vegetation and the carbon cycle as interactive elements of the climate system. *Int Geophys* 83:259–279.
50. Swindles GT, et al. (2014) Ecology of testate amoebae in an Amazonian peatland and development of a transfer function for palaeohydrological reconstruction. *Microb Ecol* 68:284–298.
51. Kelly TJ, et al. (2017) The vegetation history of an Amazonian domed peatland. *Palaeogeogr Palaeoclimatol Palaeoecol* 468:129–141.
52. Roucoux KH, et al. (2013) Vegetation development in an Amazonian peatland. *Palaeogeogr Palaeoclimatol Palaeoecol* 374:242–255.
53. Ruokolainen K, et al. (2001) On Amazonian peatlands. *Int Mire Conserv Group Newsl* 4:8–10.
54. Rammig A, et al. (2010) Estimating the risk of Amazonian forest dieback. *New Phytol* 187:694–706.
55. Roucoux KH, et al. (2017) Threats to intact tropical peatlands and opportunities for their conservation. *Conserv Biol* 31:1283–1292.